

Topological strong field physics on sub-laser cycle time scale

R. E. F. Silva^{1,2,†}, Á. Jiménez-Galán^{1,††}, B. Amorim³, O. Smirnova^{1,4}, & M. Ivanov^{1,5,6}

¹*Max-Born-Institute, Max-Born Straße 2A, D-12489 Berlin, Germany.*

²*Department of Theoretical Condensed Matter Physics, Universidad Autónoma de Madrid, E-28049 Madrid, Spain*

³*CeFEMA, Instituto Superior Técnico, Universidade de Lisboa, Av. Rovisco Pais, 1049-001 Lisboa, Portugal*

⁴*Technische Universität Berlin, Ernst-Ruska-Gebäude, Hardenbergstraße 36A, 10623 Berlin, Germany.*

⁵*Department of Physics, Humboldt University, Newtonstraße 15, D-12489 Berlin, Germany.*

⁶*Blackett Laboratory, Imperial College London, South Kensington Campus, SW7 2AZ London, United Kingdom.*

† silva@mbi-berlin.de †† jimenez@mbi-berlin.de

Sub-laser cycle time scale of electronic response to strong laser fields enables attosecond dynamical imaging in atoms, molecules and solids ¹⁻⁴. Optical tunneling and high harmonic generation ^{2,5-7} are the hallmarks of attosecond imaging in optical domain, including imaging of phase transitions in solids ^{8,9}. Topological phase transition yields a state of matter intimately linked with electron dynamics, as manifested via the chiral edge currents in topological insulators ¹⁰. Does topological state of matter leave its mark on optical tunnelling

and sub-cycle electronic response? We identify distinct topological effects on the directionality and the attosecond timing of currents arising during electron injection into conduction bands. We show that electrons tunnel across the band gap differently in trivial and topological phases, for the same band structure, and identify the key role of the Berry curvature in this process. These effects map onto topologically-dependent attosecond delays in high harmonic emission and the helicities of the emitted harmonics, which can record the phase diagram of the system and its topological invariants. Thus, the topological state of the system controls its attosecond, highly non-equilibrium electronic response to strong low-frequency laser fields, in bulk. Our findings create new roadmaps in studies of topological systems, building on ubiquitous properties of sub-laser cycle strong field response - a unique mark of attosecond science.

Intense light incident on a quantum system can drive the system's electrons far from their equilibrium within a fraction of its cycle. Accelerated by the field and by the forces inside the system, the electrons emit coherent radiation which can contain many tens (or hundreds) of harmonics of the incident light ¹. Such ultra-broad, coherent spectrum implies access to extreme time resolution of the underlying charge dynamics. It is the basis of high harmonic generation spectroscopy ^{2,3,5}, now rapidly expanding beyond atomic and molecular physics towards characterizing fundamental ultrafast processes in solids. Examples include the observation of dynamical Bloch oscillations ^{7,11,12}, band structure tomography ^{13,14}, resolving electron-hole dynamics ^{9,11,15} and light-driven phase transitions in a Mott insulator ⁸, the Peierls phase transition ⁹, or the imprint of the Berry phase on optical response ^{16,17}. Complete characterization of the emitted light, both

amplitude and spectral phase, allows one to recover time-frequency maps of the emission and thus resolve the underlying charge dynamics^{3,4}. Here, we apply these ideas to a topological insulator.

The discovery of the integer quantum Hall effect (IQHE) and its subsequent link to the so-called topological invariants of the system's bulk¹⁸, have led to the discovery of topological phases of matter. In a topological insulator, the topological phase supports states that carry currents around the insulator's edges. "Protected" by the topological invariants of the bulk, the chiral edge states are robust to perturbations, making them appealing for applications, for example in dissipationless devices or in topologically robust superconductors¹⁰. In two-dimensional (2D) materials exhibiting the IQHE, the topological invariant is the Chern number – the integral of the Berry curvature over the 2D-Brillouin zone of the filled bands.

Remarkably, in spite of extensive work on topological materials, their associated ultrafast dynamics has been hardly explored, with very few exceptions^{9,19}. Here are some of the key unanswered questions: Does the highly non-equilibrium electron dynamics in the bulk, driven by a strong laser field, encode the topological properties on the sub-laser cycle time-scale? How do the Berry curvature and the Chern number affect the first step in the nonlinear response – the field-driven injection of electrons across the bandgap? We answer these questions using the paradigmatic example of the topological insulator, the Haldane system²⁰ (Fig. 1). We show how its topological properties affect the geometry, directionality, and the attosecond timing of the injected currents. We further show that high harmonic emission encodes topologically-dependent attosecond delays induced in these currents, and that the helicities of the emitted harmonics en-

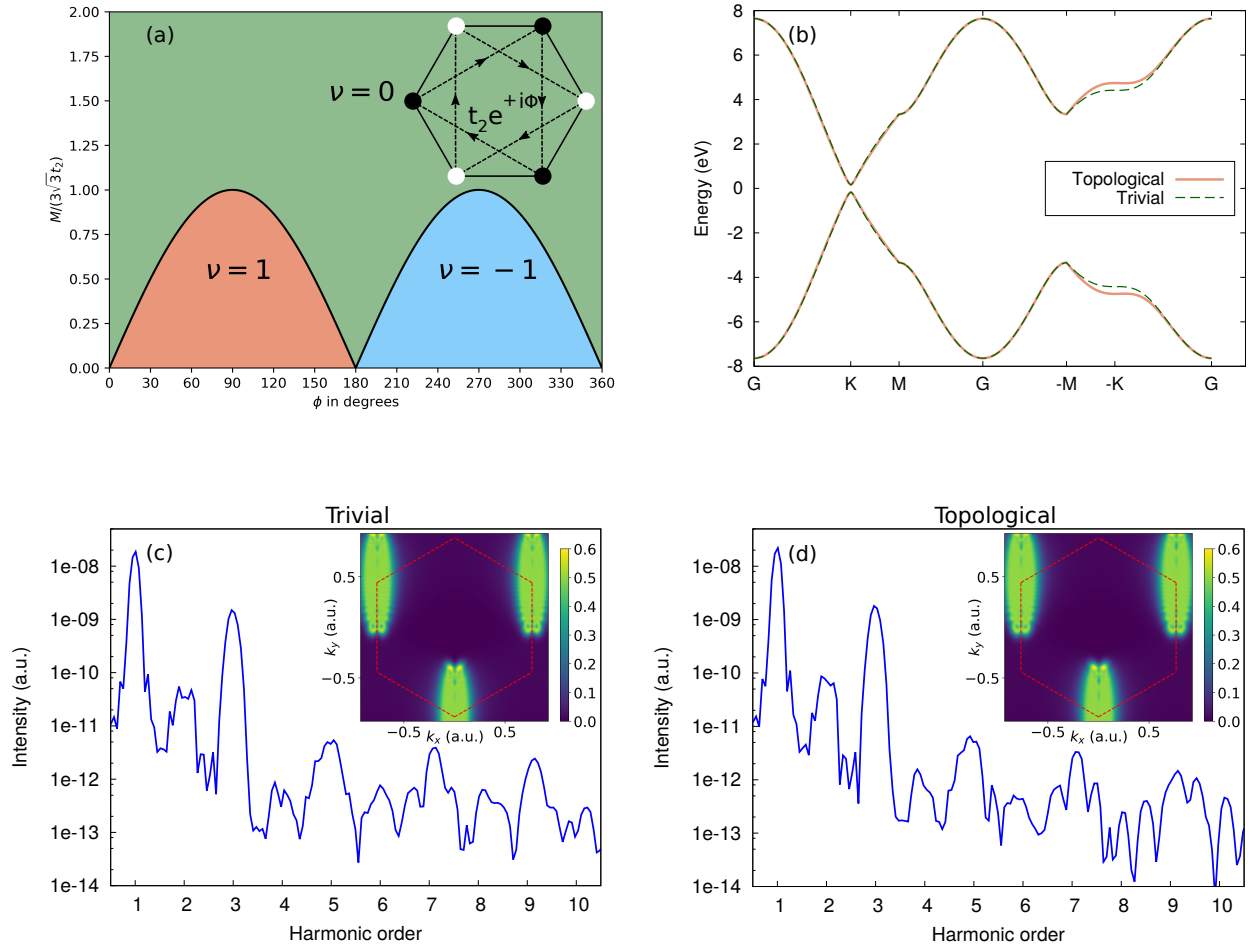


Figure 1: **The Haldane system in two phases.** (a) The phase diagram: $\nu = 0$ – trivial phase, $\nu = \pm 1$ – topological phase. Inset shows the real-space hexagonal lattice with two different atoms (black and white, on-site energies $\pm M$). Arrow lines show the second-neighbour hopping $t_2 e^{i\phi}$ with positive phase (negative phase is reversed). (b) Bulk band structures before and after the phase transition are very similar ($M/(3\sqrt{3}t_2) = 1.07$, green dashed, and $M/(3\sqrt{3}t_2) = 0.93$, orange solid). (d,e) High harmonic spectra and electron densities at the end of the pulse (as insets) at $M/(3\sqrt{3}t_2) = 1.07$ (trivial phase, (c)) and $M/(3\sqrt{3}t_2) = 0.93$ (topological phase, (d)) do not readily distinguish the two phases.

code the phase state of the system and its topological invariants. Attosecond characterization of topological effects on light-driven electron currents is a crucial step towards petahertz electronics in topological materials ²¹.

In the Haldane system, the hexagonal lattice hosts different atoms, A and B, on the adjacent sites. Their different on-site energies $\pm M$ open the bandgap at the points \mathbf{K} and $-\mathbf{K}$ of the Brillouin zone. The complex-valued second-next neighbour hopping $t_2 e^{i\phi}$ (Fig. 1a) controls the topological state. The system is a trivial insulator with zero Chern number, $\nu = 0$, if $|M/(3\sqrt{3})| > t_2 \sin \phi$, but becomes topological when $|M/(3\sqrt{3})| < t_2 \sin \phi$ (Fig. 1b), with $\nu = \pm 1$, giving rise to a non-zero Hall conductivity and the appearance of gapless edge states. This model, recently demonstrated experimentally ²², is a gateway for studying topological properties of materials such as the quantum spin Hall effect ²³ or the valley Hall effect ²⁴.

Strong field response in solids naturally emphasizes the role of the material band structure ^{7,14,25–27}. Indeed, optical tunnelling is exponentially sensitive to the bandgap, while the band structure determines the subsequent motion of electrons and holes. The transition between the trivial and the topological phases is indeed accompanied by marked changes in the bulk band structure: the gap between the valence and the conduction bands closes and then re-opens during the transition (Fig. 1c). High harmonic spectra will inevitably reflect these changes ²⁸.

Alas, they do not readily distinguish the two phases of the material. Figs. 1(c,d) show high harmonic spectra generated before and after the phase transition, using intense low-frequency field polarized linearly in the y -direction (field wavelength $\lambda = 3\mu\text{m}$, peak amplitude $E_0 = 4 \times 10^9$

V/m). The system at $t_2 = 0$ has a bandgap of 4.6 eV, chosen similar to a single layer of hexagonal boron nitride within the two band model. The band structure is very similar before and after the transition (Fig. 1b), and so is the harmonic spectrum. Attributing specific spectral features to the Berry curvature and the Chern number is hardly straightforward.

However, analogies between strong field response in atoms, molecules and solids²⁵ suggest that other key aspects of electronic structure, besides the bandstructure, should play an important role. In atoms and molecules, these are the angular momentum and the chirality of the states^{6,29,30}. We shall see how the Berry curvature takes similar role in strong field response in solids, mapping the topological state of the system onto the timing and the directionality of the injected currents. The currents control harmonic polarization and temporal structure.

Figure 2 confirms these expectations. In contrast to the harmonic spectra, the phase transition is clearly recorded in the helicities of the emitted harmonics. The helicity of the linear response (H1, first harmonic) provides a reference, while the helicities of higher harmonics (here we show H3 and H9) switch exactly at the phase transition. Tracking the helicity of H3 relative to H1 generates the phase diagram of the system (see supplementary note 1).

The key physics can be understood semiclassically. Irrespective of the specific mechanism responsible for the harmonic emission (intraband current or electron-hole recombination), harmonics are associated with the injection of charge across the bandgap. As the laser field (vector-potential $\mathbf{A}_L(t)$, field $\mathbf{E}(t) = -\partial\mathbf{A}_L/\partial t$, linearly polarized along the y axis) drives the injected electrons, changing the initial quasimomentum \mathbf{k}_i to $\mathbf{k} = \mathbf{k}(t) = \mathbf{k}_i + e\mathbf{A}_L(t)$, the non-zero Berry

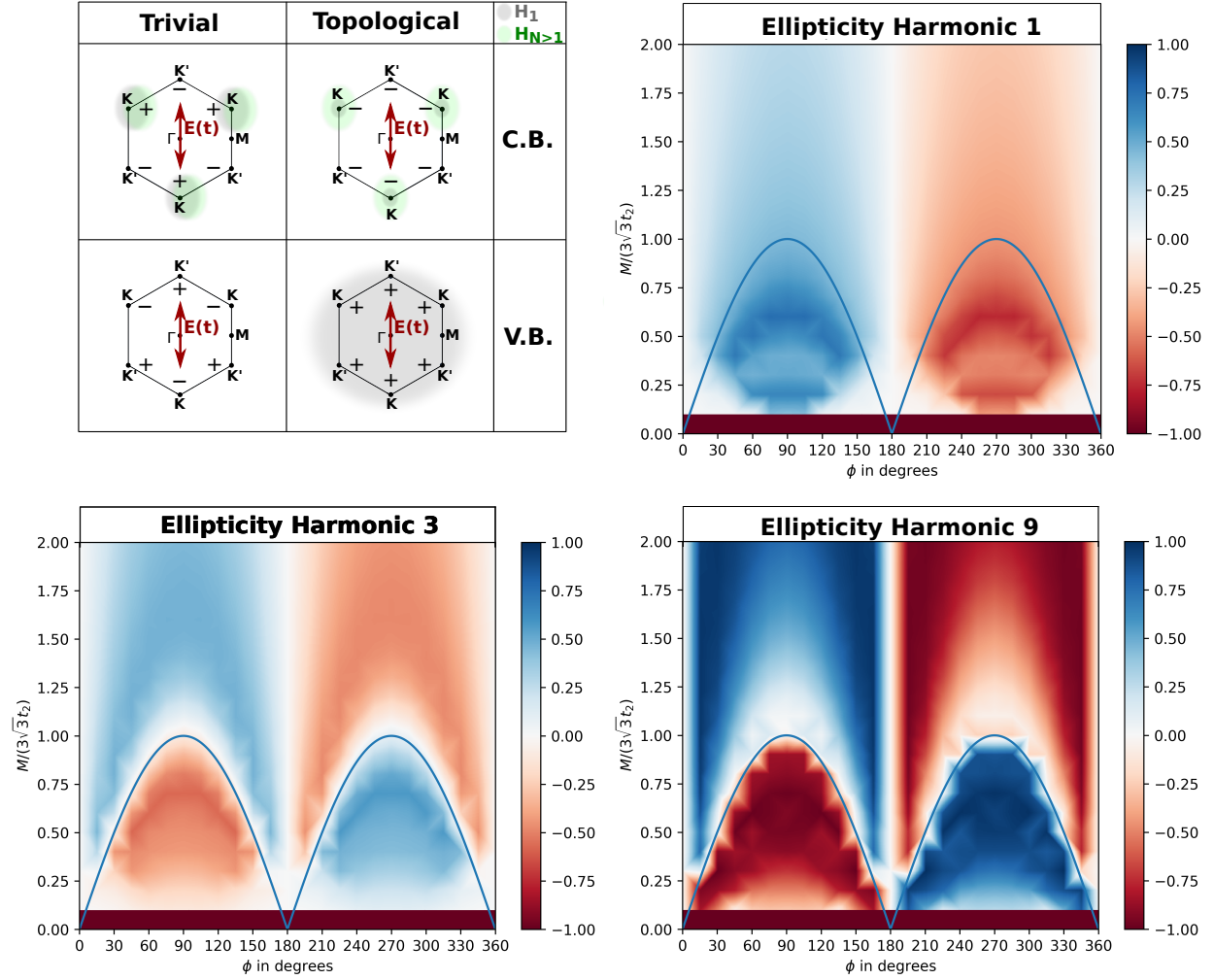


Figure 2: **Ellipticity of harmonics in topological insulators.** Top left: Scheme of the regions in the Brillouin zone probed by the first harmonic (grey shadow) and odd high harmonics (green shadow), see text for details. Ellipticity of the first (top right), third (bottom left) and ninth (bottom right) harmonics as a function of the amplitude t_2 and phase ϕ of the next-nearest neighbour hopping. The blue line indicates the topological phase transition.

curvature $\Omega(\mathbf{k})$ generates orthogonal motion in the x -direction,

$$\dot{\mathbf{r}}_n(t) = \nabla_{\mathbf{k}} \varepsilon_n(\mathbf{k}(t)) + e\mathbf{E}(t) \times \boldsymbol{\Omega}_n(\mathbf{k}(t)). \quad (1)$$

Here, n labels the band, $\varepsilon_n(\mathbf{k})$ is the band dispersion. The motion orthogonal to the field (along x) means that the emitted harmonics acquire the x component. Qualitatively, $\dot{\mathbf{r}}_n(t) \cdot \hat{e}_y$ follows the vector-potential $\mathbf{A}_L(t)$ and $\dot{\mathbf{r}}_n(t) \cdot \hat{e}_x$ follows the field $\mathbf{E}(t)$. Hence, the x and y harmonic components are $\pi/2$ out of phase, i.e. the harmonics are elliptically polarized (see Methods for a rigorous discussion).

As expected, in the trivial phase the helicities of all harmonics are the same. As the Berry curvature changes sign upon the topological transition, the anomalous current in the conduction band changes direction. Hence, the harmonics will also flip their helicity. In contrast, the response at the fundamental frequency in the topological phase does not change the helicity. The reason is that it is now dominated by the non-zero Hall conductivity of the valence band, where the Berry curvature is opposite to that in the conduction band and where most of the electrons are. Thus, the helicity of H1 is naturally opposite to that of H3 (or H9), as Fig.2 shows (see Methods for further details).

Our previous analysis has tacitly implied that, for similar bandstructures in the trivial and topological phases, the time-dependent electron densities promoted to the conduction band would also be similar. This is indeed a good first approximation, see insets in Fig. 1(c,d). As expected, the injection occurs near the peaks of the oscillating electric field ($\mathbf{A}_L(t) = 0$) and near the minima of the bandgap, i.e. in the vicinity of the \mathbf{K} points of the Brillouin zone. Once injected, the electron's

quasi-momenta cluster around $\mathbf{k}(t) = \mathbf{K} + e\mathbf{A}_L(t)$.

However, our analytical analysis of the injection step, provided in the Methods section, demonstrates that the injected densities are different in the trivial and topological phases, for the same bandstructure. Specifically, the optimal \mathbf{k} for tunnelling across the bandgap, which maximizes the injection rate, is shifted from the \mathbf{K} -point. In the parabolic band approximation near the \mathbf{K} -point, the shift orthogonal to the driving field is

$$\Delta\mathbf{k}_\perp \simeq m_\perp \mathbf{E}(t) \times \left[\Omega_c(\mathbf{k}_\parallel^{(0)}, \mathbf{k}_\perp^{(0)}) - \Omega_v(\mathbf{k}_\parallel^{(0)}, \mathbf{k}_\perp^{(0)}) \right]. \quad (2)$$

Here $\mathbf{k}_\parallel^{(0)}, \mathbf{k}_\perp^{(0)}$ are the optimal values in the absence of the Berry curvature, \parallel and \perp stand for 'parallel' and 'perpendicular' with respect to the laser polarization, Ω_v, Ω_c are the Berry curvatures in the valence and conduction bands, and m_\perp is the electron-hole effective reduced mass (Eq.(2) assumes that the band gap is above the driving laser frequency). Note that $\Delta\mathbf{k}_\perp$ has opposite sign in the trivial and the topological phases. Non-zero $\Delta\mathbf{k}_\perp$ means that, for non-zero Berry curvature, the anomalous currents reach the same region of the BZ and the same velocities at different times, shifted by $\tau \propto \Delta\mathbf{k}_\perp/\mathbf{E}$. Hence, irrespective of the harmonic emission mechanism (current- or recombination-driven), there should be a Berry curvature-induced time-delay in the emission of a given harmonic between the trivial and the topological phases, for the harmonic component orthogonal to the driving field. This delay should increase as we move away from the transition point, reflecting the increasing effective mass m_\perp .

This is confirmed by our numerical simulations. Fig. 3(a,b) show the time-frequency analysis of high harmonic emission in the trivial and topological phases (here only H3 is shown, see

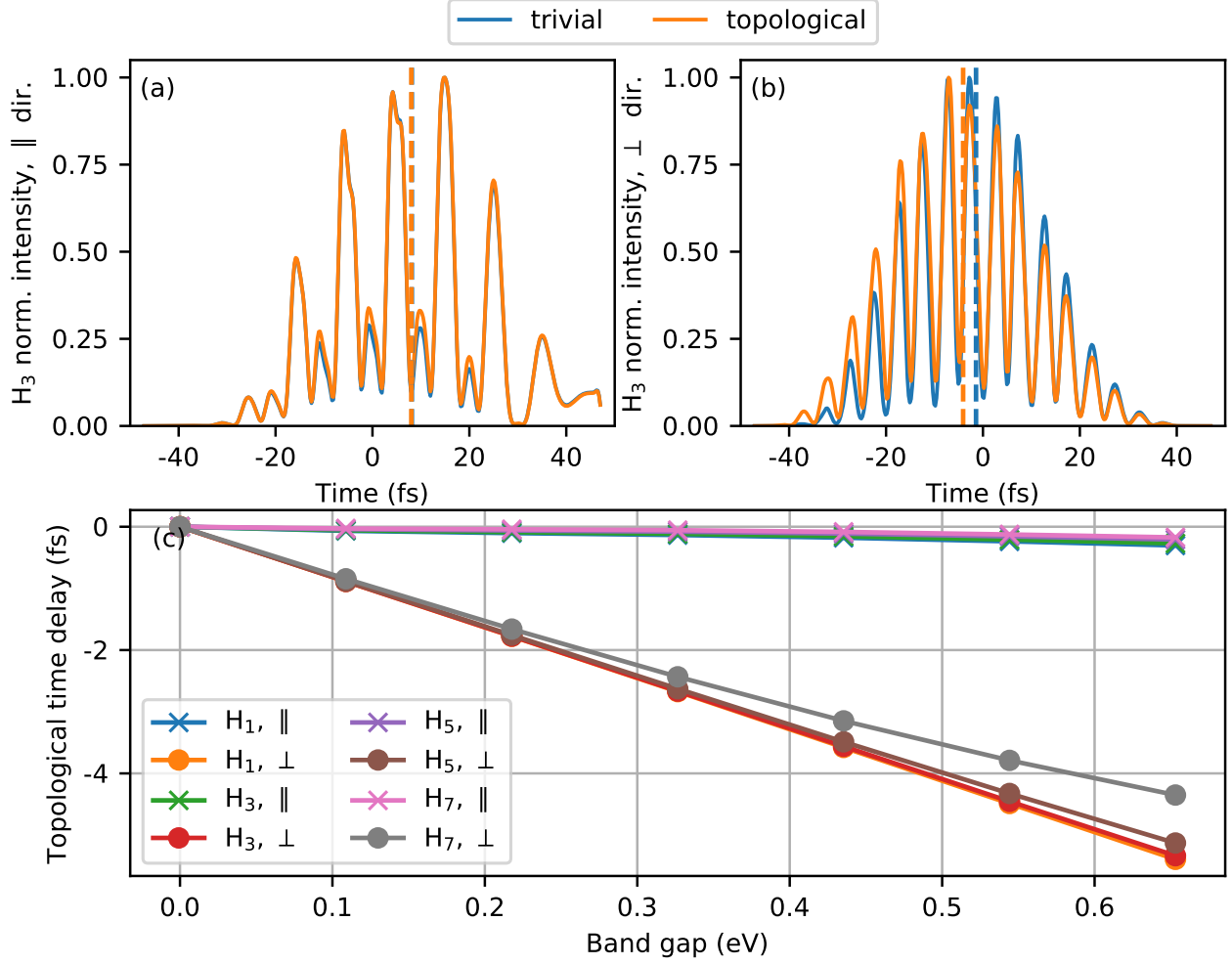


Figure 3: **Topological time delays in harmonic emission.** Time-frequency maps of the emission in the two phases shown in Fig. 1b almost overlap for the parallel component (a) but show a clear asymmetry between positive and negative times for the anomalous component (b), yielding topologically-dependent time-delays, $\tau = \langle \tau \rangle_{\text{topo}} - \langle \tau \rangle_{\text{trivial}}$, in the emission of a given harmonic (c), which vary with the bandgap. The emission time delay is defined as the weighted average, $\langle \tau \rangle = \frac{\int f(t)t dt}{\int f(t) dt}$, where $f(t)$ are the frequency-resolved time maps shown in panels (a) and (b). Panels (a) and (b) show harmonic 3 for a 0.32 eV band gap, with the blue and orange vertical dashed lines indicating the weighted average times of ionization in the trivial and topological phases, respectively.

supplementary note 2 for other high harmonics). We made sure to compare cases with virtually the same band structures in both phases (see Fig. 1(b) and supplementary note 2). For the harmonic polarization parallel to the driving field, the frequency-resolved time maps of the emission in the two phases almost overlap, signaling a negligible influence of the band structure. For the orthogonal polarization component, they visibly do not, yielding time-delays in the emission of a given harmonic exclusively linked to the topological properties of the material, Fig. 3(c).

Figs.4(a,b) show the total injected electron density integrated over the whole BZ and its Fourier transform, $\rho_{cc}(N\omega)$, for the trivial and the topological phases. It directly confirms the dependence of the injected electron density on the Berry curvature, for the same band structure. For high harmonics of the density, the topological signal, defined in the frequency domain as

$$\text{TS}_\rho(N\omega) = 2 \frac{[|\rho_{cc,top}(N\omega)| - |\rho_{cc,triv}(N\omega)|]}{[|\rho_{cc,top}(N\omega)| + |\rho_{cc,triv}(N\omega)|]} \quad (3)$$

grows with the bandgap, and, for the cases studied in this work, reaches values of 15%.

The topological dependence in the time-dependent density of the injected charges can also manifest in other observables, for example in the helicity maps of the emitted harmonics or in sudden changes in the harmonic phases (see supplementary note 3). Let us write the momentum-resolved electron density in the conduction band $\rho_{cc}(\mathbf{k}, t)$ as

$$\rho_{cc}(\mathbf{k}, t) = \rho_{cc}^{(0)}(\mathbf{k}, t; \Omega = 0) + \Delta\rho_{cc}(k, t; \Omega) \simeq \rho_{cc}^{(0)}(\mathbf{k}, t) + \Omega(\mathbf{k}) \frac{\partial \rho_{cc}}{\partial \Omega} \Big|_{\Omega=0}(k, t), \quad (4)$$

where $\rho_{cc}^{(0)}(\mathbf{k}, t)$ is the Berry curvature-independent injected density, and the second term is the correction, linear in the Berry curvature in the first order. While this additional term is small

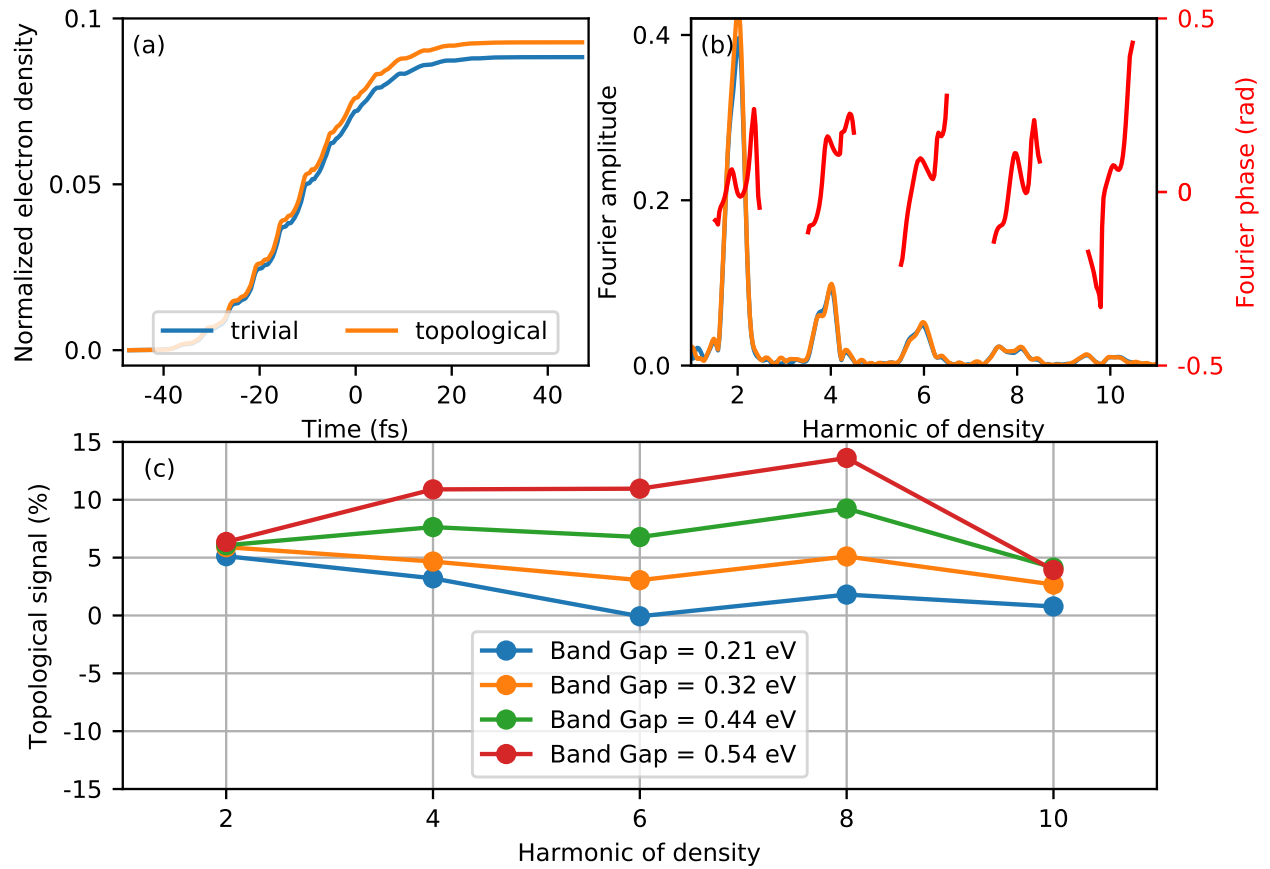


Figure 4: **Topological signal in injected currents.** Total injected electron density (a) and its Fourier transform (b), for the trivial (blue) and the topological (orange) phases with the band structures in Fig. 1b (band gap = 0.32 eV). The Fourier phase (panel b, red line) refers to the difference in the Fourier phases between the topological and trivial systems. Panel (c) shows the topological signal in the harmonic amplitude of the electron density for different band gaps.

(Fig. 1(c,d)), its contribution to the anomalous current is quadratic in Ω and does not change sign during the phase transition, in contrast to the main contribution. If the main contribution to the harmonic emission, associated with $\rho_{cc}^{(0)}(\mathbf{k}, t)$, is suppressed for a particular harmonic, the additional contribution associated with $\Delta\rho$ could become visible and the helicity of the harmonic should flip. We observe such flips in the helicity map of harmonic 5 (see supplementary note 1). This is accompanied by a sudden spectral phase jump in the harmonic line, reflecting destructive interference in the main contribution to the harmonic emission (see supplementary note 3).

Thus, the topological properties of materials manifest in the polarization and timing of the emitted harmonics. Analysis of these features allows all-optical retrieval of the complete phase diagram of the paradigmatic Chern insulator, the Haldane system, and identifies time-delays in the harmonic emission associated with the Berry curvature. Our work introduces strong-field and attosecond physics to topological materials, with high harmonic spectroscopy as a tool for characterizing topological invariants in the condensed phase, and for time resolving the ultrafast topological nonlinear response arising upon the phase transition.

References

1. Krausz, F. & Ivanov, M. Attosecond physics. *Reviews of Modern Physics* **81**, 163–234 (2009).
URL <https://link.aps.org/doi/10.1103/RevModPhys.81.163>.
2. Baker, S. *et al.* Probing proton dynamics in molecules on an attosecond time scale. *Science* **312**, 424–427 (2006). URL <http://science.sciencemag.org/>

content/312/5772/424. <http://science.sciencemag.org/content/312/5772/424.full.pdf>.

3. Shafir, D. *et al.* Resolving the time when an electron exits a tunnelling barrier. *Nature* **485**, 343 EP – (2012). URL <http://dx.doi.org/10.1038/nature11025>.
4. Hohenleutner, M. *et al.* Real-time observation of interfering crystal electrons in high-harmonic generation. *Nature* **523**, 572 EP – (2015). URL <http://dx.doi.org/10.1038/nature14652>.
5. Smirnova, O. *et al.* High harmonic interferometry of multi-electron dynamics in molecules. *Nature* **460**, 972 EP – (2009). URL <http://dx.doi.org/10.1038/nature08253>.
6. Eckart, S. *et al.* Ultrafast preparation and detection of ring currents in single atoms. *Nature Physics* (2018). URL <https://doi.org/10.1038/s41567-018-0080-5>.
7. Ghimire, S. *et al.* Observation of high-order harmonic generation in a bulk crystal. *Nature Physics* **7**, 138 EP – (2010). URL <http://dx.doi.org/10.1038/nphys1847>.
8. Silva, R. E. F., Blinov, I. V., Rubtsov, A. N., Smirnova, O. & Ivanov, M. High-harmonic spectroscopy of ultrafast many-body dynamics in strongly correlated systems. *Nature Photonics* (2018). URL <https://doi.org/10.1038/s41566-018-0129-0>.
9. Bauer, D. & Hansen, K. K. High-harmonic generation in solids with and without topological edge states. *Physical Review Letters* **120**, 177401– (2018). URL <https://link.aps.org/doi/10.1103/PhysRevLett.120.177401>.

10. Hasan, M. Z. & Kane, C. L. Colloquium. *Reviews of Modern Physics* **82**, 3045–3067 (2010).
URL <https://link.aps.org/doi/10.1103/RevModPhys.82.3045>.
11. Schubert, O. *et al.* Sub-cycle control of terahertz high-harmonic generation by dynamical bloch oscillations. *Nature Photonics* **8**, 119 EP – (2014). URL <http://dx.doi.org/10.1038/nphoton.2013.349>.
12. Luu, T. T. *et al.* Extreme ultraviolet high-harmonic spectroscopy of solids. *Nature* **521**, 498 EP – (2015). URL <http://dx.doi.org/10.1038/nature14456>.
13. Vampa, G. *et al.* All-optical reconstruction of crystal band structure. *Physical Review Letters* **115**, 193603– (2015). URL <https://link.aps.org/doi/10.1103/PhysRevLett.115.193603>.
14. Tancogne-Dejean, N., Mücke, O. D., Kärtner, F. X. & Rubio, A. Impact of the electronic band structure in high-harmonic generation spectra of solids. *Physical Review Letters* **118**, 087403– (2017). URL <https://link.aps.org/doi/10.1103/PhysRevLett.118.087403>.
15. McDonald, C. R., Vampa, G., Corkum, P. B. & Brabec, T. Interband bloch oscillation mechanism for high-harmonic generation in semiconductor crystals. *Physical Review A* **92**, 033845– (2015). URL <https://link.aps.org/doi/10.1103/PhysRevA.92.033845>.
16. Liu, H. *et al.* High-harmonic generation from an atomically thin semiconductor. *Nature Physics* **13**, 262 EP – (2016). URL <http://dx.doi.org/10.1038/nphys3946>.

17. Luu, T. T. & Wörner, H. J. Measurement of the berry curvature of solids using high-harmonic spectroscopy. *Nature Communications* **9**, 916 (2018). URL <https://doi.org/10.1038/s41467-018-03397-4>.
18. Thouless, D. J., Kohmoto, M., Nightingale, M. P. & den Nijs, M. Quantized hall conductance in a two-dimensional periodic potential. *Physical Review Letters* **49**, 405–408 (1982). URL <https://link.aps.org/doi/10.1103/PhysRevLett.49.405>.
19. Reimann, J. *et al.* Subcycle observation of lightwave-driven dirac currents in a topological surface band. *Nature* **562**, 396–400 (2018). URL <https://doi.org/10.1038/s41586-018-0544-x>.
20. Haldane, F. D. M. Model for a quantum hall effect without landau levels: Condensed-matter realization of the "parity anomaly". *Physical Review Letters* **61**, 2015–2018 (1988). URL <https://link.aps.org/doi/10.1103/PhysRevLett.61.2015>.
21. Garg, M. *et al.* Multi-petahertz electronic metrology. *Nature* **538**, 359 EP – (2016). URL <http://dx.doi.org/10.1038/nature19821>.
22. Jotzu, G. *et al.* Experimental realization of the topological haldane model with ultracold fermions. *Nature* **515**, 237 EP – (2014). URL <http://dx.doi.org/10.1038/nature13915>.
23. Kane, C. L. & Mele, E. J. \mathbb{Z}_2 topological order and the quantum spin hall effect. *Physical Review Letters* **95**, 146802– (2005). URL <https://link.aps.org/doi/10.1103/PhysRevLett.95.146802>.

24. Mak, K. F., McGill, K. L., Park, J. & McEuen, P. L. The valley hall effect in mos2 transistors. *Science* **344**, 1489–1492 (2014). URL <http://science.sciencemag.org/content/344/6191/1489>. <http://science.sciencemag.org/content/344/6191/1489.full.pdf>.
25. Vampa, G. & Brabec, T. Merge of high harmonic generation from gases and solids and its implications for attosecond science. *Journal of Physics B: Atomic, Molecular and Optical Physics* **50**, 083001 (2017). URL <http://stacks.iop.org/0953-4075/50/i=8/a=083001>.
26. Ndabashimiye, G. *et al.* Solid-state harmonics beyond the atomic limit. *Nature* **534**, 520 EP – (2016). URL <http://dx.doi.org/10.1038/nature17660>.
27. Hawkins, P. G., Ivanov, M. Y. & Yakovlev, V. S. Effect of multiple conduction bands on high-harmonic emission from dielectrics. *Physical Review A* **91**, 013405– (2015). URL <https://link.aps.org/doi/10.1103/PhysRevA.91.013405>.
28. Chacón, A. *et al.* Observing topological phase transitions with high harmonic generation. *arXiv:1807.01616* (2018). URL <https://arxiv.org/abs/1807.01616>.
29. Barth, I. & Smirnova, O. Nonadiabatic tunneling in circularly polarized laser fields: Physical picture and calculations. *Physical Review A* **84**, 063415– (2011). URL <https://link.aps.org/doi/10.1103/PhysRevA.84.063415>.
30. Cireasa, R. *et al.* Probing molecular chirality on a sub-femtosecond timescale. *Nature Physics* **11**, 654 EP – (2015). URL <http://dx.doi.org/10.1038/nphys3369>.

Data availability. The data that support the findings of this study are available from the corresponding author upon request.

Acknowledgements R.E.F.S. and M.I. acknowledge support from EPSRC/DSTL MURI grant EP/N018680/1. A.J.G and M.I. acknowledge support from the DFG QUTIF grant IV 152/6-1. O.S. acknowledge support from the DFG SPP 1840 “Quantum Dynamics in Tailored Intense Fields” project SM 292/5-1; and MEDEA project, which has received funding from the European Union’s Horizon 2020 research and innovation programme under the Marie Skłodowska-Curie grant agreement No 641789. B.A. received funding from the European Union’s Horizon 2020 research and innovation programme under grant agreement No. 706538.